

Out of equilibrium dynamics in the bidimensional spin-ice model

DEMIAN LEVIS¹ and LETICIA F. CUGLIANDOLO¹

¹ *Université Pierre et Marie Curie - Paris 6, Laboratoire de Physique Théorique et Hautes Energies, 4, Place Jussieu, Tour 13, 5ème étage, 75252 Paris Cedex 05, France*

PACS 74.40.Gh – Fluctuation phenomena, nonequilibrium processes

PACS 75.10.Hk – Ising model, magnetic ordering

PACS 75.40.Mg – Computer modeling and simulation of magnetic critical points

Abstract – We study the dynamics of $2d$ spin-ice following a quench from a fully disordered initial condition (equilibrium at infinite temperature) into its disordered, ferromagnetic and anti-ferromagnetic phases. We analyze the evolution of the density of topological defects and we show that these take finite density over very long periods of time in all kinds of quenches. We identify the leading mechanisms for the growth of domains in the ordered phases and we evaluate the (anisotropically) growing lengths involved in dynamic scaling.

In a large class of condensed-matter systems the tendency to local ordering is hampered by constraints. Frustration entails, typically, a non-vanishing entropy at zero temperature.

The prototypical example is *water ice* for which this zero point entropy has been measured in the 30s [1]. Pauling explained this feature with a model in which the O atoms occupy the vertices of a coordination four lattice and exactly two H atoms are near while the other two H atoms are shifted away from each vertex [2]. The large degeneracy of such locally electro-neutral ground states gives rise to the zero point entropy.

A residual entropy has also been measured in frustrated magnets [3,4] such as $\text{Ho}_2\text{Ti}_2\text{O}_7$ [5]. In these *spin-ice* samples, the relevant interacting degrees of freedom are classical Ising spins located at the nodes of a pyrochlore lattice and aligned with the local axis connecting two corner-sharing tetrahedra [4]. Each tetrahedron can be seen as a vertex in a $3d$ lattice taking one out of sixteen possible configurations. The energy is locally minimized when two spins point inward and two outward verifying the ice rule or zero-divergence condition for the magnetic moments carried by the spins. The other ten ‘defects’ have a magnetic charge $q = \vec{\nabla} \cdot \vec{S}$. Experimentally, the statistical weights of the vertices can be tuned by applying uniaxial pressure that break the isotropy of the ice-model but preserve the Z_2 symmetry [6]. Magnetic fields along different crystallographic axes can also be used to modify the vertex weights.

Two dimensional spin-ice samples have also been pro-

duced in the laboratory. On the one hand, high magnetic fields project the system onto $2d$ Kagome slices [7]; on the other hand, ‘artificial’ spin-ice on a $2d$ square lattice can be manufactured with lithography [8,9]. Although the magnetic moments in artificial spin-ice are *a priori* athermal, an effective thermodynamics can be generated with applied rotating magnetic fields [10,11]. More recently, thermal excitations have also been engineered in these samples [12].

In recent years, research in this field has been boosted by the exciting proposal that topological defects, in the form of magnetic monopoles and their attached Dirac strings, could be observed in spin-ice samples [13–18]. Following the proposal in [13] experiments have shown evidence for this kind of excitation [16–18]. Reaction-diffusion arguments have been used to estimate the density of defects in the disordered phase of $3d$ spin ice [15]. As far as we know no studies of dynamics in the ordered phases nor beyond this simple modeling have been performed.

Here we choose a different approach to address the dynamics of spin-ice models. For the sake of simplicity we focus on thermal quenches in the $2d$ square lattice spin ice model built as a stochastic extension of the celebrated *6 vertex model* of statistical mechanics [19]. We use a rejection-free continuous-time Monte Carlo (MC) algorithm [20], with local spin-flip updates and non-conserved order parameter, that allows for thermally-activated creation of defects. The longest time reached with this method, once translated in terms of usual MC sweeps, is of the order of 10^{16} MCs, a scale practically unreachable

with usual Metropolis algorithms. This allows us to identify the equilibrium phase diagram and to analyze different dynamic regimes. Our dynamic results are manifold. We reproduce known facts of the dynamics of spin ice samples, as the existence of long-lived metastable states although with no need of long-range interactions. We prove that the dynamics after a quench into the FM and AF phases conforms to the domain-growth scaling picture [21] and we identify the anisotropic growing lengths. We derive a large number of new results that, we propose, should be realized experimentally [22]. Our findings should also be of interest to the integrable systems community.

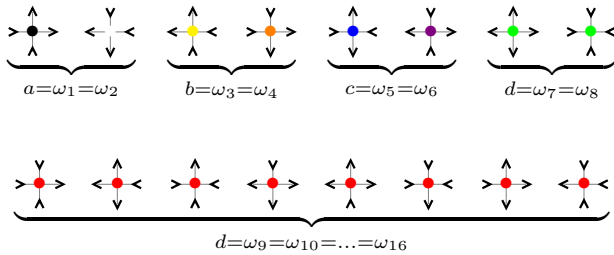


Fig. 1: (Color online.) The sixteen vertex configurations on the $2d$ square lattice and their weights. The first six vertices verify the ice-rule. The next pair completes the eight-vertex model and have charge $q = \pm 2$. The last eight vertices have charge $q = \pm 1$. This color code is used in Fig. 5.

The model. We consider an $L \times L$ square lattice with unit spacing and periodic boundary conditions and we vary the linear size L from 10 to 300. Each edge is occupied by an arrow modeled as a binary variable $S = \pm 1$. We assign a Boltzmann weight $\omega_k \propto e^{-\beta \epsilon_k}$ to each of the $k = 1, \dots, 2^4$ four-arrow vertex configurations. The energy is $H = \sum_{k=1}^{16} \epsilon_k n_k$, where n_k is the number of vertices of type k . We set $\omega_1 = \omega_2 = a$, $\omega_3 = \omega_4 = b$, $\omega_5 = \omega_6 = c$ for the ice-rule vertices and $\omega_7 = \omega_8 = d$, $\omega_9 = \dots = \omega_{16} = d$ for the 2-fold and 1-fold defects, respectively, ensuring invariance under reversal of all arrows (see Fig. 1). Henceforth we measure the weights in units of c .

Equilibrium properties. In the $2d$ six-vertex model defects are forbidden. A host of exact equilibrium properties of this model were derived with the Bethe Ansatz and *via* mappings to random matrix theory, algebraic combinatorics (domino tilings) and crystal growth [19]. Depending on the weight of the vertices the system sets into a quasi long-range ordered paramagnetic (PM) or disordered (D), two ferromagnetic (FM) and one anti-ferromagnetic (AF) phases separated by different transition lines. The four phases of the six-vertex model ($d = 0$) are characterized by the parameter $\Delta_6 = (a^2 + b^2 - 1)/(2ab)$ [19]. (i) For $\Delta_6 > 1$ and $a > b + 1$ the vertices of type 1 and 2 (type 3 and 4 for $b > a + 1$) are statistically favored and the system is frozen into one of its two symmetric ground states with perfect FM order and no low energy excitations. At

$|a_c^{FM} - b| = 1$, i.e. $\Delta_6 = 1$, there are two first-order phase transition. (ii) For $-1 < \Delta_6 < 1$ the system is quasi long-range ordered. The ice-rule is strong enough to prevent full de-correlation at any temperature. At $a_c^{AF} = 1 - b$, i.e. $\Delta_6 = -1$ there is a Kosterlitz-Thouless (KT) phase transition. (iii) For $\Delta_6 < -1$ vertices of type 5 and 6 are favored and the system orders into an AF state populated by low energy excitations. The phase diagram is shown in Fig. 2 with solid (red) lines. This scenario is modified by the ice-rule breaking vertices ($d \neq 0$) as we discuss below.

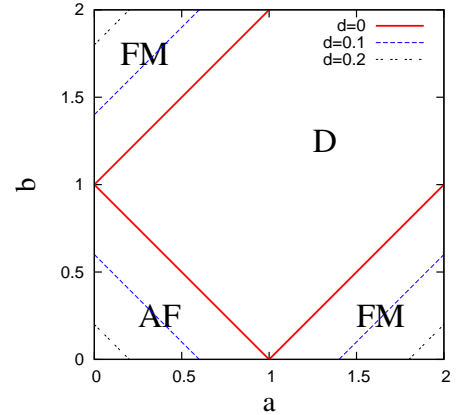


Fig. 2: (Color online.) (a, b) -plane projection of the sixteen-vertex model phase diagram. The solid (red) lines are the six-vertex model first-order transition between disordered (D) and ferromagnetic (FM) phases, and KT transition between disordered (D) and antiferromagnetic (AF) phase. The second-order transition lines for $d \neq 0$ are shown with dashed (blue and black) lines.

The $2d$ sixteen-vertex model is isomorphic to the Ising model on the checkerboard lattice with many-body interactions [23]. While this model is integrable for a special set of parameters for which the equivalent Ising model has two-body interactions only, none of these special cases corresponds to our choice of parameters. We then used MC simulations to elucidate the equilibrium phase diagram and statistical properties of relatively small samples. We set the origin of coordinates on a vertex. The indices (α, β) are the coordinates of each vertex and $((2\alpha + 1)/2, \beta)$ and $(\alpha, (2\beta + 1)/2)$ locate the mid-points of the right- and up- pointing bonds. We checked equilibration with standard criteria; in particular, we verified (i) that the density of vertices stabilizes at long times at the same value starting the evolution from very different initial configurations; (ii) that the spatially local two-time correlation function depends on the time difference only. These tests will be shown in [24]. After verifying equilibration in this way we computed: (i) The absolute staggered magnetization per spin defined as $M_{\pm} = (\langle |m_{\pm}^x| \rangle + \langle |m_{\pm}^y| \rangle) / 2$ with $L^2 m_{\pm}^x = \sum_{(\alpha, \beta) \in A} S_{(2\alpha+1)/2, \beta} \pm \sum_{(\alpha, \beta) \in B} S_{(2\alpha+1)/2, \beta}$ and its counterpart m_{\pm}^y . In the expressions for m we divided the lattice into two sub-lattices A and B such that $\alpha + \beta$ is even and odd, respectively. The \pm signs al-

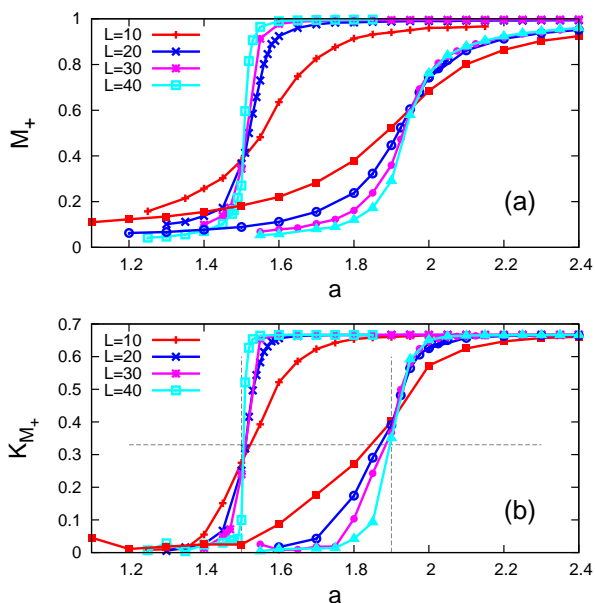


Fig. 3: (Color online.) Study of the FM transition. (a) Magnetization per spin M_+ and (b) magnetization cumulant K_{M_+} as a function of a for $b = 0.5$, $d = 10^{-5}$ (the group of curves on the left) and $d = 0.1$ (the ones on the right), and several L given in the key. The crossing points of K_{M_+} determine $a_c(b, d)$. The vertical dotted (black) lines are the critical values predicted by $|\Delta_{16}| = 1$. The horizontal dotted level is $1/3$.

low one to distinguish between FM and AF order. (ii) The fourth-order cumulant $K_{M_{\pm}} = (K_{m_{\pm}^x} + K_{m_{\pm}^y})/2$ with $K_{m_{\pm}^x} = 1 - \langle (m_{\pm}^x)^4 \rangle / 3 \langle (m_{\pm}^x)^2 \rangle$. $\langle \dots \rangle$ denotes an average over independent runs. In Fig. 3 (a) we show M_+ for $b = 0.5$ and two values of d as a function of a . $L = 10, \dots, 40$ and we averaged over $10^3 - 10^4$ samples. The variation of the magnetization as a function of a shows a sharp jump at $a = 1.5$ for $b = 0.5$ and $d = 0$, as expected for a first order phase transition. For $d > 0$ the curve takes a sigmoid form that gets wider (less step-like) for increasing d . The intersection point appears at larger values of a for larger values of d . These features suggest that the transition to the FM phase is continuous, occurs at larger values of a , and that there are fluctuations in the ordered state. The crossing of K_{M_+} at height $1/3$ (dotted horizontal line) for several values of L shown in Fig. 3 (b) determines $a_c(b, d)$. Finite size scaling will be discussed in [24]. Consistently with a second-order phase transition, K_{M_+} remains positive for all L and the energy cumulant (not shown) converges to zero. The analysis of the staggered magnetization and its cumulant demonstrates that the AF transition no longer belongs to the KT universality class and also becomes second-order as soon as $d \neq 0$ [24]. The projection of the critical lines onto the (a, b) -plane are shown in Fig. 2 with dashed (blue and black) lines. For $d = 10^{-5}$ they agree, within our numerical accuracy, with the exact critical lines for the six-vertex model. For increasing d the extent of the PM phase increases. The

excitation properties are radically modified by the relaxation of the ice-rule: the paramagnetic (PM) phase loses its quasi long-range order and the FM state admits excitations [24]. These conclusions are in agreement with exact computations on the eight- [19,23] and sixteen- [23] vertex models for special values of the parameters. We conjecture that the phase diagram is characterized by the *anisotropy parameter* $\Delta_{16} = [a^2 + b^2 - c^2 - (4d)^2] / [2(ab + c(4d))]$. The PM phase corresponds to the parameter space submanifold with $|\Delta_{16}| < 1$, the FM phase to $\Delta_{16} > 1$ and the AF phase to $\Delta_{16} < -1$ in agreement with the fact that the transition lines are parallel to the six-vertex model ones. A similar displacement of the critical lines was found in spin-ice on the Husimi tree [25].

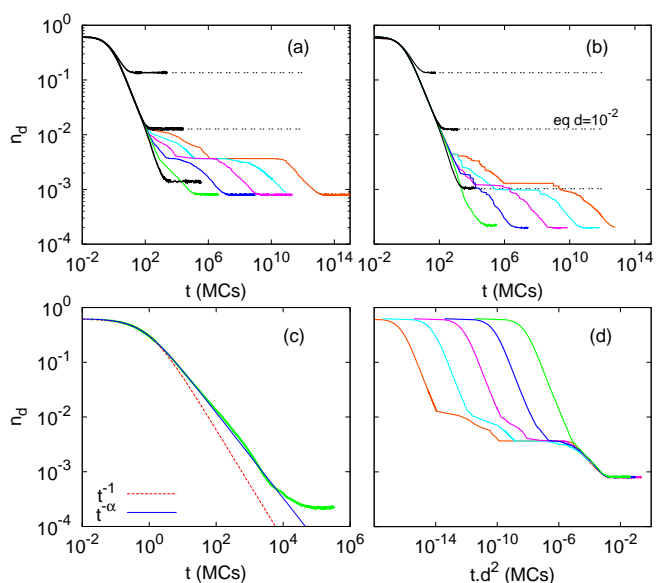


Fig. 4: (Color online.) Time-dependent density of defects, $n_d(t)$, after a quench from $T \rightarrow \infty$ to $a = b = 1$ and $d = 10^{-1}, 10^{-2}, \dots, 10^{-8}$. (a) $L = 50$ and (b) $L = 100$. The black curves are for $d = 10^{-1}, 10^{-2}, 10^{-3}$. The gray (color) curves are for smaller values of d decreasing from left to right. (c) Short time behavior in the case $d = 10^{-4}$ and $L = 100$ confronted to the decay $\rho_0/(1 + \Omega t)$ (dashed curve) [15] and the fit $\rho_0/(1 + \Omega t)^\alpha$ with $\alpha = 0.78$ (blue plain curve). (d) Test of scaling with $t d^2$ for systems with $L = 50$.

Quench dynamics. We now turn to the dissipative stochastic dynamics of an equilibrium initial configuration at $a = b = d = 1$ (i.e. $T \rightarrow \infty$) after a quench to sets of parameters in the (i) disordered, (ii) FM, and (iii) AF phases. In case (i) the system should equilibrate easily but the question remains as to whether it gets blocked in metastable states with a large density of defects. In cases (ii) and (iii) the interactions between the spins, mediated by the choice of vertex weights, should create ordered domains, FM or AF. The quantitative characterization of growth in the ordering processes is given by two possibly different growing lengths extracted from correlation functions along orthogonal directions \parallel and \perp that we identify.

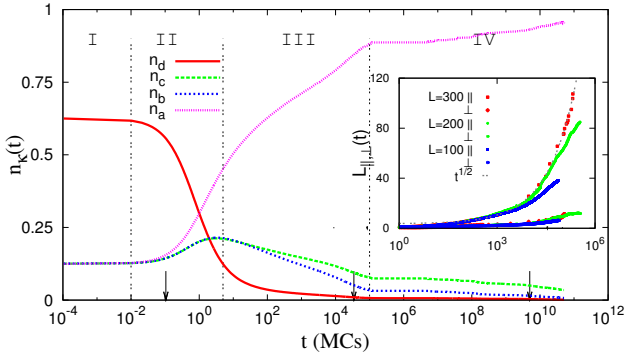


Fig. 5: (Color online.) FM ordering. Upper panel: time evolution of the density of vertices with weight a, b, c, d for $a = 5$, $b = 1$, $d = 10^{-5}$ and $L = 100$ averaged over 300 samples. The snapshots are typical configurations at the dates indicated by the arrows. Black/white points are vertices $1/2$ and the rest are shown in gray (color) scale. Inset: time-dependence of the longitudinal (upper curves) and transverse (lower curves) growing lengths for three system sizes, $L = 100, 200, 300$. A fit to $t^{1/2}$ is shown with a dotted black line.

(i) *Quench into the disordered (D) phase.* Figure 4 displays the time-dependent density of defects, $n_d(t)$, defined as the number of vertices of type 7-16 divided by L^2 , after an infinitely rapid quench to $a = b = 1$ and $d = 10^{-8}, \dots, 10^{-1}$ of samples with linear size $L = 50$ (a) and $L = 100$ (b). These data have been averaged over 10^3 runs.

For large d (black dark curves) $n_d(t)$ quickly saturates to its equilibrium value. Numerical estimates of the equilibrium density of defects, n_d^{eq} , for $d = 10^{-1}, 10^{-2}, 10^{-3}$ are shown with dotted black lines. As expected n_d^{eq} is an intensive quantity that increases with d . It does not depend upon the system size for $L \geq 50$ and $d > 10^{-3}$.

For small d ($\lesssim 10^{-4}$) the systems do not reach equilibrium within the simulated time-window. After a first decay, $n_d(t)$ gets frozen at approximately constant values before relaxing, in a much longer time-scale, to a configuration in which only two defects are present in our small samples. Note that in order to distinguish the d -dependent equilibrium values for these very small d s one would need to equilibrate much larger samples. Unfortunately, the special purpose loop algorithm devised for the 6 vertex model does not apply to our generalized case. For our working sizes we see asymptotes taking the value $2/L^2$ on average.

The initial decay is fitted by a $\rho_0/(1 + \Omega t)^\alpha$ power-law

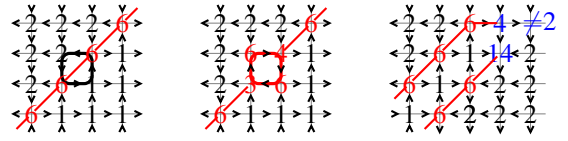


Fig. 6: (Color online.) Interfaces between FM domains. Local vertices and spins on the bonds are shown. Left panel: diagonal wall (red solid line). Central panel: a ‘loop’ fluctuation on the plaquette highlighted in the left panel. Right panel: a b corner vertex cannot be neighbor of an a -vertex, explaining the presence of strings.

decay with $\alpha \simeq 0.78$ over three orders of magnitude in t and n_d , as shown in panel (c) in Fig. 4. The power-law is shown with a solid blue line in the figure together with the data for $d = 10^{-4}$ and $L = 100$. This law is different from the simple t^{-1} decay found with a mean-field approximation to a diffusion-reaction model shown with a dashed red line in the same figure [15].

The decay is next arrested at a metastable density of defects $n_d^{pl} \approx 10/L^2$. The plateau lasts longer for smaller d and its height is roughly independent of d . This feature is reminiscent of what was found numerically in dipolar spin-ice although contrary to the modeling in [15] our model does not have long-range interactions. At the entrance to the plateau the system has between 3 and 4 times more defects of type 7-8 than those of type 9-16 which are only 2 or 3. Therefore, in the final decay from the plateau to the asymptotic value $n_d \approx 2/L^2$ the remaining doubly charged defects have to disappear. This may be due to two kinds of processes. In the first case, two defects of type 7 and 8 meet to produce two singly (and oppositely) charged defects with no energetic gain. The total density of defects remains constant after this reaction. An example of the second case is a reaction in which a defect of type 7 (charge $q = 2$) meets one of type 14 (charge $q = -1$) to produce a defect of type 10 (charge $q = 1$) and a spin-ice vertex with no charge. In terms of a reaction-diffusion model this corresponds to $2q + (-q) \rightarrow q + 0$ and, consequently, an energetic gain. Note that the number of single charged defects has not been modified in this process but the number of doubly charged defects diminished and so did the total number of defects. In both cases the remaining defects need to diffuse, a process with no energetic cost, to find a partner and annihilate. From inspection of the individual runs and the densities of single and doubly charged defects we see that the second process is favored, as also suggested by the energetic gain. This regime is characterized by a scaling of the dynamic curves with the scaling variable td^2 [26] as shown in Fig. 4 (d) for the $L = 50$ data.

(ii) *Quench into the FM phase.* We choose $a = 5$, $b = 1$ and $d = 10^{-5}$, favoring vertices with weight a . In Fig. 5 we present the density of vertices, $n_\kappa(t)$, with $\kappa = a, b, c, d$, in a log-linear scale. The evolution is illustrated with three

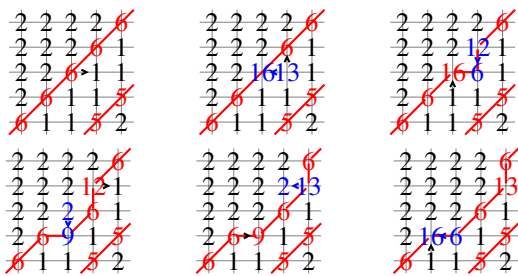


Fig. 7: (Color online.) Schematic representation of FM stripe motion. Vertices on each site are specified. Diagonal (red) lines delimit domains of opposite magnetization. Black arrows indicate the spins that flip to get the new configuration (represented in blue after the flip).

configurations at instants shown with vertical arrows. Domains grow anisotropically and we choose the \parallel and \perp directions to be parallel and perpendicular to the diagonal joining the lower-left and upper-right corners in the pictures, respectively. During a short transient ($t \lesssim 0.01$ MCs) all densities remain roughly constant (regime I). Suddenly, a large number of defects are transformed into divergence-free vertices by a few single spin-flips: n_d decays while n_a , n_b and n_c increase (regime II) independently of a [24]. A typical configuration at this stage is the left-most snapshot and there is no visual ordering as corroborated by the small values taken by $L_{\parallel, \perp}$ and displayed in the inset in a log-linear scale for three values of the system size, $L = 100$, $L = 200$ and $L = 300$. Subsequently the system sets into a slow relaxation regime in which the dominant mechanism is the one of growing anisotropic domains with FM order, see the central snapshot (regime III); n_c depend upon a and there are as many domains with $m^{x,y} = 1$ (vertices 1) as $m^{x,y} = -1$ (vertices 2) respecting symmetry. In this regime L_{\parallel} grows faster than L_{\perp} and tends to saturate to an L -dependent value when the stripes are fully formed. For the largest sample size, $L = 300$, our numerical data are consistent with a $t^{1/2}$ growth that is shown with a dotted black line. Instead order in the \perp direction has not yet percolated. The full equilibration of the sample needs the percolation of order in the \perp direction which is achieved by a still much slower mechanism (regime IV).

A better understanding of the processes involved in the ordering dynamics is reached from the analysis of the snapshots. (a) Domain walls are made of c -vertices and plaquettes of divergence-free vertices, as shown in the left and central panels in Fig. 6, respectively. The latter are ‘loop’ fluctuations in which all the spins on the plaquette are sequentially flipped. Interfaces between FM states tend to be parallel to the main diagonal, which one depending on which FM phase one quenches into. (b) Quasi-one-dimensional paths made of b and c vertices (loop fluctuation can be attached to them) act as bridges between two domains of the same type and run through a region with

the opposite order. These structures are similar to the ones found in the kinetically constrained spiral model [27]. In order to further increase the density of a -vertices and develop the FM order the domain walls and bridges have to be eliminated. The latter disappear first via the following mechanism. ‘Corners’ made of b (or, less commonly, d) vertices sit on a curved domain wall. Such b vertices cannot be surrounded by more than two type 1 or 2 vertices (only defects can, see the third panel in Fig. 6). The string progressively disappears eaten by the attached domains that grow from the corner or, alternatively, it is first cut by the creation of two defects and the two strands subsequently shrink, an extremely slow process. Once the path has been eliminated one is left with two defects sitting on the walls of the now detached domains, that move along the interface and eventually annihilate with their anti-partner. Once parallel bands are created (third configuration in Fig. 5) the mechanism in Fig. 7 takes over (regime IV). After the creation of a pair of defects on the interface, the sequence of steps in the figure shrink the vertex 1 stripe on a time scale that diverges with L .

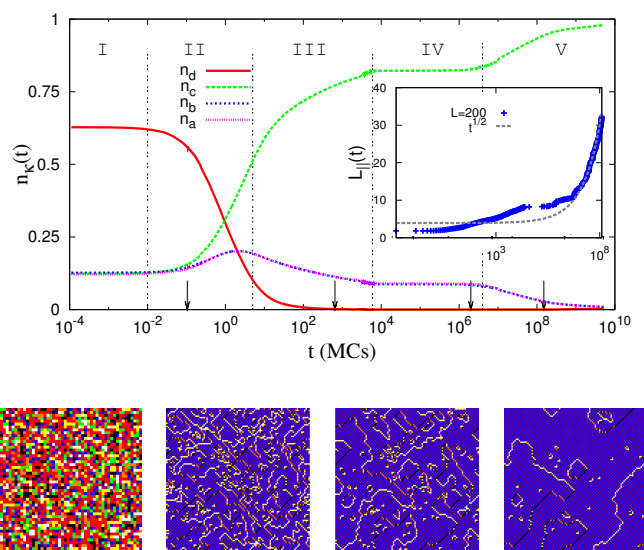


Fig. 8: (Color online.) AF ordering. Time evolution of the density of vertices in a system with $L = 100$ after a quench to $a = 0.1$, $b = 0.1$, $d = 10^{-5}$ averaged over 300 runs. Inset: the time-dependent growing length L_{\parallel} confronted to $t^{1/2}$ (dotted black line). Typical configurations are shown.

(iii) *Quench into the AF phase.* The evolution of the vertex population is shown in the main panel in Fig. 8 for $a = b = 0.1$ and $d = 10^{-5}$. Similarly to what found in the FM quenches, in regime I all densities remain approximately constant. This is followed by regime II with a rapid annihilation of defects into divergence-free vertices. The creation of a , b and c -vertices occurs with a rate that depends on a while, surprisingly, n_d does not, at least within our numerical accuracy. In regime III the system

increases the AF order by growing domains of staggered magnetization ± 1 with c vertices. Since a is very close to b for our choice of parameters, domains are quite isotropic and the growing length are, within numerical accuracy, $t^{1/2}$. Regime IV follows next and it is characterized by a strong slowing-down although there is no obvious extended structure blocking the evolution. In regime V the system finally reaches equilibrium. The relevant elementary moves in each regime will be discussed in [24].

We presented a numerical study of the quench dynamics of 2d spin-ice. In this Letter we established the main statics and dynamical properties of this model: equilibrium phase diagram and relaxation dynamics after thermal quenches. No study of frustrated magnet existed in the literature such complete. We demonstrated the existence of long-lived metastable states with an excess of topological defects in a model with no long-range interactions, cfr. [15]. We showed that the dynamics after quenches into the FM and AF phases proceed by coarsening of equilibrium domains. More details will be presented in an extended publication [24]. Our results should motivate new experimental studies of the dynamics in frustrated magnets and possibly motivate researchers in the integrable systems community to try to adapt their very powerful techniques to deal with dynamical issues.

* * *

We thank R. Borzi, C. Castelnovo, L. D. C. Jaubert and S. Grigera for useful discussions. This work was financially supported by ANR-BLAN- 0346 (FAMOUS).

REFERENCES

- [1] GIAUQUE W. F. and STOUT J. W., *J. Am. Chem. Soc.* , **58** (1936) 1144.
- [2] PAULING L., *J. Chem. Phys.* , **57** (1935) 2680.
- [3] BALENTS L., *Nature* , **464** (2010) 199.
- [4] BRAMWELL S. T., GINGRAS M. J. P. and HOLDSWORTH P. C. W., *Spin Ice in Frustrated spin systems*, edited by DIEP H. T., (World Scientific) 2004 Ch. 7.
- [5] HARRIS M. J. *et al.*, *Phys. Rev. Lett.* , **79** (1997) 2554.
- [6] MITO M. *et al.*, *J. Magn. Magn. Mat.* , **310** (2007) 432.
- [7] FENNEL T. *et al.*, *Nature Phys.* , **3** (2007) 566.
- [8] WANG R. F. *et al.*, *Nature* , **439** (2006) 303.
- [9] MÖLLER G. and MOESSNER R., *Phys. Rev. Lett.* , **96** (2006) 1.
- [10] NISOLI C. *et al.*, *Phys. Rev. Lett.* , **98** (2007) 1.
- [11] BUDRIKIS Z., POLITI P. and STAMPS R. L., *Phys. Rev. Lett.* , **105** (2010) 017201.
- [12] KAPAKLIS V., ARNALDS U. B. and HARMAN-CLARKE A., *arXiv:1108.1092* , (2011) .
- [13] CASTELNOVO C., MOESSNER R. and SONDHI S. L., *Nature* , **451** (2008) 42.
- [14] JAUBERT L. D. C. and HOLDSWORTH P. C. W., *Nature Phys.* , **5** (2009) 258.
- [15] CASTELNOVO C., MOESSNER R. and SONDHI S. L., *Phys. Rev. Lett.* , **104** (2010) 107201.
- [16] MORRIS D. J. P. *et al.*, *Science* , **326** (2009) 411.
- [17] SLOBINSKY D. *et al.*, *Phys. Rev. Lett.* , **105** (2010) 267205.
- [18] MENGOTTI E. *et al.*, *Nature Phys.* , **7** (2011) 68.
- [19] BAXTER R. J., *Exactly solved models in statistical mechanics* (Dover) 1982.
- [20] BARKEMA G. T. and NEWMAN M. E. J., *Monte Carlo Methods in Statistical Mechanics* (Oxford University Press) 1999.
- [21] BRAY A. J., *Adv. in Physics* , **51** (2002) 481.
- [22] WILLS A. S. *et al.*, *Phys. Rev. B* , **62** (2000) 9264.
- [23] LIEB E. H. and WU F. Y., *Two-dimensional ferroelectric models in Phase transitions and critical phenomena Vol. 1*, edited by DOMB C. and LEBOWITZ J. L., (Academic Press) 1972 Ch. 8.
- [24] LEVIS D. and CUGLIANDOLO L. F., *In preparation* , (2011) .
- [25] JAUBERT L. D. C., *Topological Constraints and Defects in Spin Ice* Ph.D. thesis ENS Lyon (2009).
- [26] CASTELNOVO C., private communication (2011).
- [27] CORBERI F. and CUGLIANDOLO L. F., *J. Stat. Mech. Theor. Exp.* , (2009) P09015.